Supporting Material for

Ras G domain lacks intrinsic propensity to form dimers

Elizaveta A Kovrigina[#], Azamat R Galiakhmetov[#], Evgenii L Kovrigin*

Supporting Figures

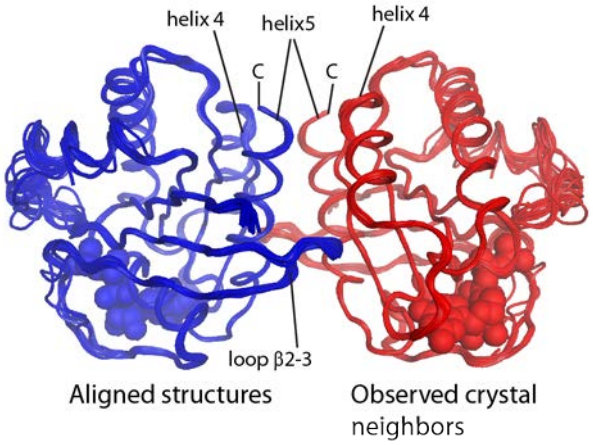


```
                                                                 D  E
H-Ras MTEYKLVVVGAGGVGKSALTIQLIQNHFVDEYDPTIEDSYRKQVVIDGETCLLDILDTAG 60
N-Ras MTEYKLVVVGAGGVGKSALTIQLIQNHFVDEYDPTIEDSYRKQVVIDGETCLLDILDTAG 60
K-Ras MTEYKLVVVGAGGVGKSALTIQLIQNHFVDEYDPTIEDSYRKQVVIDGETCLLDILDTAG 60
      ************************************************************
      |         |         |         |         |         |         |
      1         10        20        30        40        50        60
H-Ras QEEYSAMRDQYMRTGEGFLCVFAINNTKSFEDIHQYREQIKRVKDSDDVPMVLVGNKCDL 120
N-Ras QEEYSAMRDQYMRTGEGFLCVFAINNSKSFADINLYREQIKRVKDSDDVPMVLVGNKCDL 120
K-Ras QEEYSAMRDQYMRTGEGFLCVFAINNTKSFEDIHHYREQIKRVKDSEDVPMVLVGNKCDL 120
      **************************:*** **: ***********:*************
      |         |         |         |         |         |         |
      61        70        80        90        100       110       120
              Q/H   R/K               D       R  R
H-Ras AARTVESRQAQDLARSYGIPYIETSAKTRQGVEDAFYTLVREIRQHKLRKLNPPDESGPG 180
N-Ras PTRTVDTKQAHELAKSYGIPFIETSAKTRQGVEDAFYTLVREIRQYRMKKLNSSDDGTQG 180
K-Ras PSRTVDTKQAQDLARSYGIPFIETSAKTRQGVDDAFYTLVREIRKHKEKMSKDGKKKKKK 180
      .:***:::**::**:*****:***********:**********::: : : ..
      |         |         |         |         |         |         |
      121       130       140       150       160       170       180

H-Ras CMSCKCVLS 189
N-Ras CMGLPCVVM 189
K-Ras SK-TKCVIM 188
      . **:
      |
      181
```

Figure S1. Illustration of the "crystallographic" dimers in Ras and analysis of sequence conservation at the dimer interface.
(Top panel) Alignment of crystal structures of Ras illustrating the conserved "crystallographic" dimer. The backbone alignment of 17 structures (PDB ID: 5p21, 1gnr, 1jah, 1jai, 1rvd, 2cl0, 3l8y, 3l8z, 3v4f, 4l9s, 4l9w, 121p, 221p, 421p, 621p, 721p, and 821p) is shown in blue; in red—the observed crystallographic neighbor (generated using symmetry operations in Pymol(46)). C-alpha trace is shown as a tube. C-termini of each monomer are indicated. Atoms of the guanine nucleotides are represented as spheres (one nucleotide for each group of structures). Six crystal structures belong to the H 3 2 space group; the rest—to P 3_2 2 1.
(Bottom panel) Multiple sequence alignment of human Ras isoforms H-Ras, N-Ras, and K-Ras (NCBI accession # AAM12630, AAM12633, and NP_004976, respectively) performed with ClustalW(47). The residues involved in salt bridges at the crystallographic dimer interface are boxed.

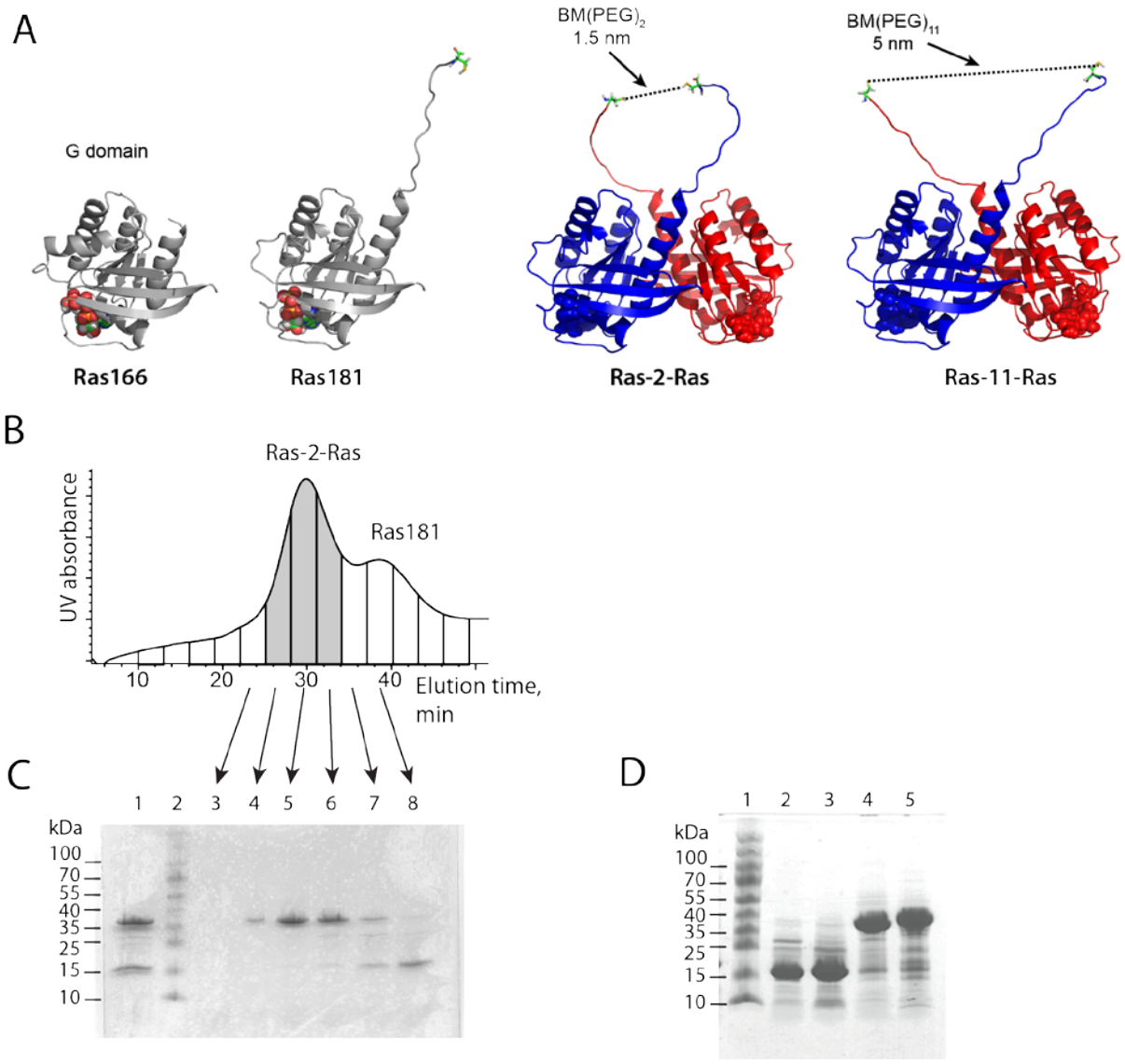

Figure S2. (A) Protein models utilized in this study: Ras166, the truncated G domain of H-Ras, residues 1-166; Ras181, the cytosolic portion of the full-length H-Ras, residues 1-181; Ras-2-Ras and Ras-11-Ras, the inverted-tandem conjugates of two Ras181 molecules. Nucleotides are shown as spheres; C-terminal cysteines are sticks. The model of Ras166 is based on PDB ID 5P21 (residues 1-166; contains "crystallographic dimer"). The Ras181 is modeled using 1Q21 (residues 1-171 with extended helix 5; no "dimer"). To create the full-length model of the "crystallographic dimer", two 1Q21 structures were aligned to the dimeric structure from 5P21. The unstructured C-terminal peptides, residues 172-181, were added to 1Q21 in Pymol and modeled in conformations to show that there are no steric restrictions to form the dimeric structure with either 1.5 or 5 nm distance between C-terminal cysteines. The BM(PEG) linkers are schematically shown with dashed lines. Drawing is approximately to scale. (**B**) The size-exclusion chromatography profile of the conjugation reaction mixture utilizing $BM(PEG)_2$. The conjugate and monomer peaks are labeled with 'Ras-2-Ras' and 'Ras181', respectively. The profile for the Ras-11-Ras reaction was qualitatively similar. (**C**) SDS-PAGE analysis of the reaction mixture prior to injection on the size-exclusion column (lane 1), and fractions from the

elution profile (lanes 3-8) in panel A. Lane 2, PageRuler Prestained Protein Ladder (Fermentas, SM0671). The Ras-2-Ras fractions (lanes 4, 5, and 6) were further concentrated to prepare Ras-2-Ras samples; the Ras181 fractions (lanes 7 and 8) were discarded. (**D**) Analysis of purity of the final protein preparations. The lanes were intentionally overloaded to visualize residual contaminating proteins. Lane 1, PageRuler Prestained Protein Ladder; Lane 2, first R181 preparation; Lane 3, second R181 preparation; Lane 4, Ras-2-Ras sample; Lane 5, Ras-11-Ras sample.

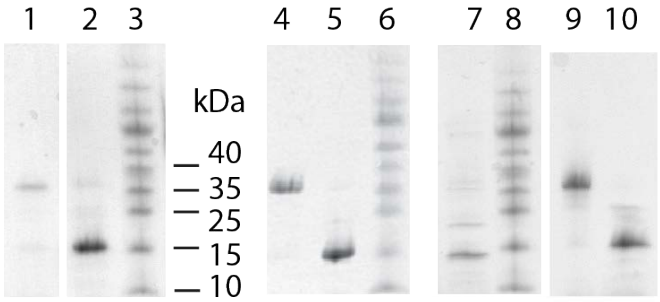

Figure S3. Confirmation of integrity of the fluorescence and NMR samples after all measurements. The NMR samples were loaded directly; the samples from the anisotropy decay measurements were concentrated by precipitation with trichloroacetic acid to allow for visualization with the Coumassie staining. Lane 1, Ras-2-Ras fluorescence sample; lane 2, Ras181 fluorescence sample; lanes 3, 6, and 8; PageRuler Prestained Protein Ladder as in Figure S2; lane 4, Ras-11-Ras fluorescence sample; lane 5, Ras181 fluorescence sample from the second protein preparation; lane 7, Ras166 fluorescence sample; lane 9; Ras-2-Ras NMR sample; lane 10, Ras181 NMR sample.

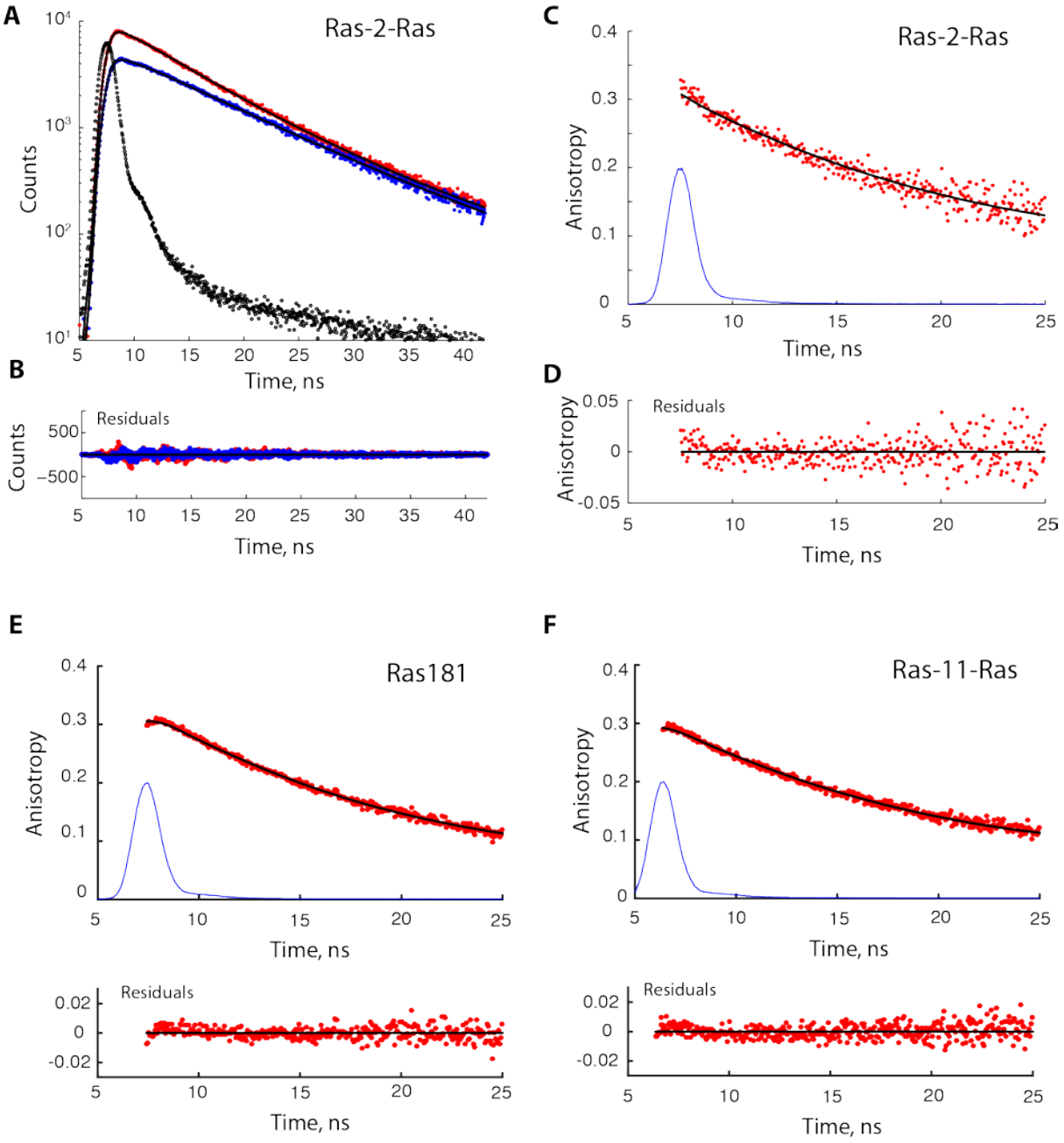

Figure S4. Representative analysis of time-domain fluorescence measurements of Ras-2-Ras conjugate (Panels A-D), Ras181 (Panel E), and Ras-11-Ras conjugate (Panel F). The proteins were complexed with mant-GDP. Excitation was provided by pulsed LED at 365 nm; polarized decays were detected at 440 nm with 24 nm slits. Buffer conditions: 20 mM HEPES pH 7.2, 5 mM $MgCl_2$, and 1 mM DTT at 20°C. **(A)** Polarized intensity decays of Ras-2-Ras at 11 μM: parallel component, red circles; perpendicular component, blue circles; best-fit curves, black lines. Acquisition time was 40 minutes per polarizer orientation. Instrument response function is shown with black circles. **(B)** Residuals from fitting of the parallel and perpendicular components. The best fit parameters for the reconstructed isotropic decay were: a_1 = 1.59, t_1 =

0.056 ns, a_2 = 0.69, t_2 = 5.55 ns, a_3 = 1.16, t_3 = 8.88 ns. The goodness-of-fit parameter χ^2 is 1.95—slightly elevated due to the hardware artifact, a high-frequency oscillation with the 2.5 ns period, observable in the early time points. **(C)** Representation of the fitting results for Ras-2-Ras in the form of anisotropy decays: experimental anisotropies calculated using the parallel and perpendicular decay data, red circles; anisotropy decay model including contribution of scattered light and one rotational correlation time, black line. Instrument response function, a blue line, is shown for time referencing. Best-fit parameters: r_0 = 0.29 [0.27 - 0.30], θ = 16.2 [14.9 - 17.6] ns; the 95% confidence intervals are shown in parentheses. **(D)** Deviation of the anisotropy decay model from the experimental anisotropy decay. (**E**) Anisotropy decay of Ras181 at 8 µM, averaged from 23 hours of total acquisition time. Best fit parameters: r_0 = 0.33 [0.32 - 0.34], θ = 14.9 [14.2 - 15.5] ns. (**F**) Anisotropy decay of Ras-11-Ras conjugate at 5 µM, 17 hours total acquisition time. Best fit parameters: r_0 = 0.30 [0.28 - 0.30], θ = 15.4 [14.5 - 16.2] ns.

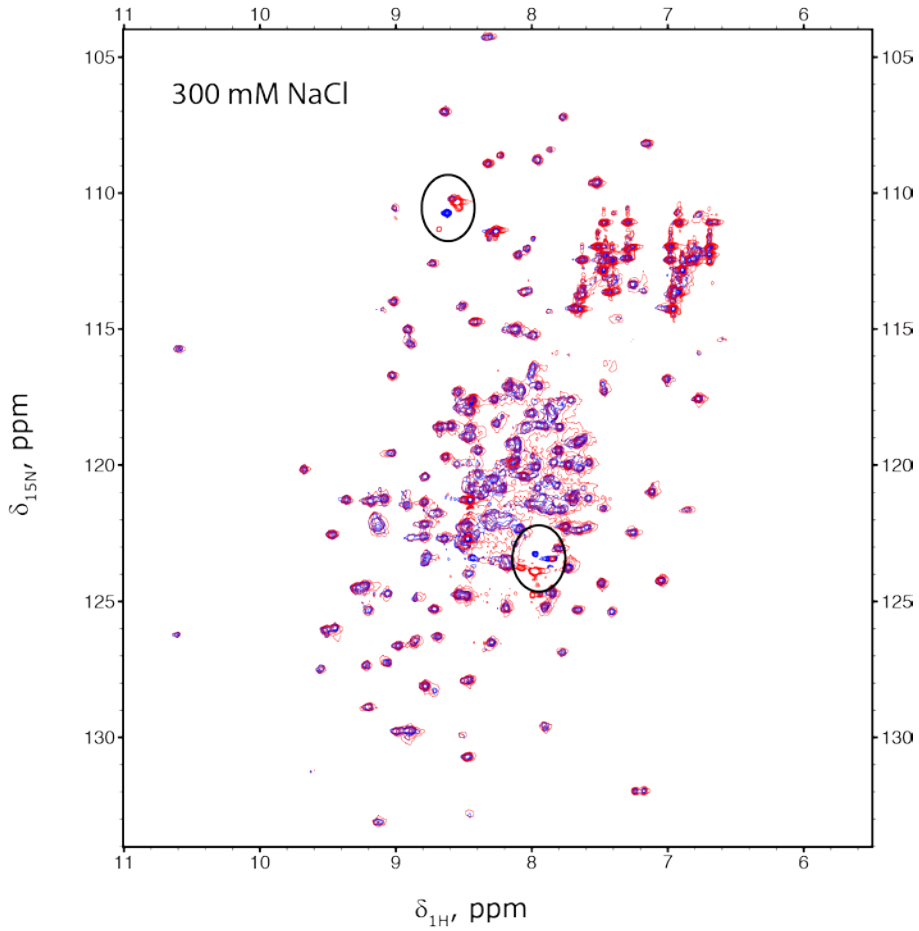

Figure S5. Overlay of ^{15}N-^{1}H HSQC NMR spectra for Ras-2-Ras (red) onto the Ras181 (blue) at high ionic strength (300 mM NaCl) at 20^{o}C.

Table S1. Summary of fitted rotational correlation times of Ras181 and Ras conjugates complexed with mant-GDP. Buffer conditions: 20 mM HEPES pH 7.2, 5 mM $MgCl_2$, and 1 mM DTT with variable concentrations of NaCl. Best-fit values of the rotational correlation time are given along with the 95% confidence intervals obtained from the Jacobian matices. Determination of the error intervals using χ^2 surfaces was not possible due the hardware artifact (Figure S4.B) that resulted in inflated χ^2 values not adequately sensitive to variation of the model parameters.

Temperature	**θ_{Ras181}, ns**	**$\theta_{Ras\text{-}2\text{-}Ras}$, ns**	**$\theta_{Ras\text{-}11\text{-}Ras}$, ns**
no NaCl			
20 ^{o}C	13.1 [12.3 - 13.9][1] 14.9 [14.2 - 15.5][2] 12.5 [12.0 - 13.1][3]	16.2 [14.9 - 17.6]	15.4 [14.5 - 16.2]
25 ^{o}C	11.4 [10.7 - 12.1][1]	13.1 [12.0 - 14.1]	
37 ^{o}C	8.5 [8.0 - 9.1][1] 8.5 [8.1 - 8.9][2]	10 [9 - 12]	9.8 [9.2 - 10.3]
150 mM NaCl			
20 ^{o}C	13.5 [12.6 - 14.5][1]	17.1 [15.7 - 18.6]	18.3 [16.9 - 19.8]
25 ^{o}C	11.8 [10.9 - 12.6][1]	15.5 [14.2 - 16.8]	
37 ^{o}C	8.7 [8.1 - 9.3][1] 9.2 [8.6- 9.8][2]	10.4 [9.5 - 11.2]	9.8 [9.2 - 10.3]
300 mM NaCl			
20 ^{o}C	15.8 [14.6 - 17.0][1]	18.2 [16-20]	20.7 [18.6 - 22.7]
25 ^{o}C	13.0 [12.0 - 14.0][1]	16.2 [13.9 - 18.5]	
37 ^{o}C	8.6 [8.3 - 9.3][1] 8.9 [8.4 - 9.3][2]	10.0 [9.0 - 11.0]	10.5 [9.9 - 11.1]

[1]) The first preparation of Ras181, which served as a source for Ras-2-Ras preparation;
[2]) The second preparation of Ras181, which served a source for Ras-11-Ras preparation;
[3]) Repeated measurement using the sample from the first preparation of Ras181.

Estimation of rotational correlation times for the Ras conjugates

Anisotropy decays of ellipsoids of revolution

The calculation of rotational correlation times outlined below is based on theory of anisotropy decays reviewed by Kawski (48) and Lakowicz (49). The anisotropy decay of the ellipsoid of revolution is composed of three contributions corresponding to decays of anisotropy projections onto the principal axes of the ellipsoid, r_i (50, 51). Each contribution decays with its corresponding rotational correlation time, θ_i:

$$r(t) = r_1 \exp(-t/\theta_1) + r_2 \exp(-t/\theta_2) + r_3 \exp(-t/\theta_3) \qquad \text{Eq. S1}$$

The rotational correlation times are related to coefficients of rotational diffusion of the ellipsoid around long and short axes, $D_{\|}$ and $D_{\perp}$:

$$\begin{aligned} \theta_1 &= (D_{\|} + 5D_{\perp})^{-1} \\ \theta_2 &= (4D_{\|} + 2D_{\perp})^{-1} \\ \theta_3 &= (6D_{\perp})^{-1} \end{aligned} \qquad \text{Eq. S2}$$

Coefficients of rotational diffusion of ellipsoids of revolution with the axial ratio $\rho = a/b$ are given by the following equations:

$$\frac{D_{\|}}{D} = \frac{3\rho(\rho - S)}{2(\rho^2 - 1)} \qquad \frac{D_{\perp}}{D} = \frac{3\rho\left[(2\rho^2 - 1)S - \rho\right]}{2(\rho^4 - 1)} \qquad \text{Eq. S3}$$

where *D* is the rotational diffusion coefficient of a sphere of equivalent volume, and *S* is expressed as

$$S = (\rho^2 - 1)^{-1/2} \ln\left[\rho + (\rho^2 - 1)^{1/2}\right] \qquad \text{Eq. S4}$$

for the *prolate* ellipsoid ($\rho > 1$), and

$$S = (1 - \rho^2)^{-1/2} \arctan\left[(1 - \rho^2)^{1/2} / \rho\right] \qquad \text{Eq. S5}$$

for the *oblate* ellipsoid ($\rho < 1$), respectively.

Technical note Expression for *S* of a prolate ellipsoid (Eq. S4) comes from (48) (Eq. 157) and was incorrectly reproduced in (49) (Eq. 12.23). In turn, the equation for *S* of the oblate ellipsoid (Eq. S5) contains a typo in (48) (Eq. 156), which was corrected by Lakowitz (Eq. 12.24). Equations S4 and S5 represent correct versions of the expressions.

Rotational diffusion coefficient of a spherical protein particle is calculated using Stokes-Einstein equation:

$$D = \frac{RT}{6\eta M(\bar{\nu} + h)} \qquad \text{Eq. S6}$$

where *M* is a molecular weight of the protein in gram/mol, η - viscosity of solvent in centipoise (cP), $\bar{\nu}$ - specific volume, ml/gram, *h* - hydration in ml/gram. Typical values of the specific volume and hydration parameters for proteins are $\bar{\nu} = 0.73$ ml/g and *h* = 0.4 ml/gram (49).

Viscosity of water at the experimental temperatures was estimated using data from (52) to be $\eta = 1.00$ cP at 20°C , 0.89 cP at 25 °C, and 0.69 cP at 37 °C.

Rotational correlation times of the G domain

Based on the crystallographic structure the Ras G domain may be represented as a prolate ellipsoid of revolution with the axial ratio of approximately 1.3. Using Equations S2-S6 we can estimate rotational correlation times for Ras166 (Table S2).

Table S2. Expected rotational correlation times of the prolate ellipsoid of revolution with the molecular weight of the isolated G domain (residues 1-166, 18.9 kDa) and axial ratio of $\rho = 1.3$ as well as for the sphere of equivalent volume.

Temperature	θ_1	θ_2	θ_3	θ_{sphere}
20 °C	9.34 ns	8.49 ns	9.67 ns	8.8 ns

The important observation here is that the axial ratio of 1.3 represents a small degree of asymmetry giving rise to very closely spaced correlation times, which would be difficult to resolve by fitting experimental anisotropy decays (49). Therefore, we should expect the G domain to be reasonably characterized by a single rotational correlation time of approx. 9 ns.

Experimental anisotropy decay for the isolated G domain of H-Ras (residues 1-166) is shown in Figure S6. The data only supported fitting of one correlation time—fitting with two correlation times resulted in statistically insignificant values. The best-fit correlation time was 9.0 ns (95% confidence interval of 8.5 to 9.4 ns). This is remarkably similar to the predicted correlation times in Table S2.

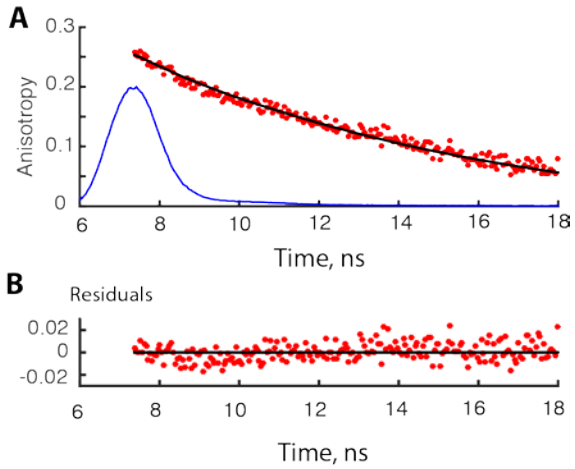

Figure S6. The anisotropy decay of the mant-GDP in complex with H-Ras residues 1-166 at 20°C in presence of 20 mM HEPES pH 7.2, 5 mM $MgCl_2$, and 1 mM DTT. (A) Experimental anisotropy values are red circles; fitted curve is black line; IRF is shown as blue line for time referencing. (B) Residuals of fit.

Calculations of rotational correlation times for the Ras181 construct (G domain + unstructured C-terminal tail) are not straightforward because the C-terminal tail is flexible. Comparison of the isolated G domain value of 9.0 [8.5, 9.4] ns with experimental values of 13-15 ns for Ras181 at the same temperature and salt indicates that extended helix 5 and the unstructured C-terminal peptide add hydrodynamic drag. However, addition of the C-terminal peptide did not significantly increase degree of asymmetry based on our observations that anisotropy decays for Ras181 did not support fitting with more than one rotational correlation time.

We may offer a speculation why Ras181 is still well approximated by a sphere of slightly bigger size than Ras166 despite the C-terminal tail. It is important to note that rotational diffusion should not be pictured as spinning in one direction. Instead, rotational diffusion is a sequence of reorientations with frequently changed directions and random angles induced by vigorous collisions with solvent molecules. A flexible chain extending from the rigid core of the protein may be expected to "wrap around" multiple ways thus impacting the hydrodynamic size but less—asymmetry of the overall structure.

Relationship between rotational diffusion of monomeric and dimeric Ras structures

Similar reasoning may be applied to the Ras-Ras dimer to anticipate that the flexible loop connecting the C-terminal residues of the G domains will also slow down rotational diffusion. Since the "tail" in Ras181 and the "loop" in Ras conjugates have similar hydrophilic character and lack stable structure, they are likely to impact rotational diffusion to a similar degree.

We hypothesized that we can estimate the expected *relative increase* of rotational correlation times from Ras181 to Ras-2-Ras or Ras-11-Ras by evaluating the increase of calculated correlation times from Ras166 to the "crystallographic dimer". Using the axial ratio of 2 estimated from the dimers in crystal structures, we calculated their rotational correlation times and the corresponding ratios to the correlation times of a single G domain (Table S3).

Table S3. Rotational correlation times of the prolate ellipsoid of revolution approximating "crystallographic" Ras dimer (37.8 kDa, axial ratio of $\rho = 2.0$) at 20 ^{o}C. Dimer/monomer ratios are calculated using corresponding values from Table S2.

	θ_1	θ_2	θ_3
Rotational correlation time, ns	23.17	16.81	26.52
Ratios to monomer's values	**2.5**	**2.0**	**2.7**

Conclusion

If Ras-2-Ras and Ras-11-Ras constructs, indeed, contain G domains forming the "crystallographic dimer" the measured rotational correlation time should exceed the one measured for the Ras181 monomer by a factor ranging from 2 to 2.7. Using the experimental

value of 13 ns for Ras181 at 20^{o}C, we expect the rotational correlation times of the Ras dimers to be in the range from 26 to 35 ns. At 37^{o}C, we expect Ras dimers tumble with 17 to 23 ns correlation times. These ranges are depicted in Figure 1 with black bars.